Structure of Cr monolayer on Ag(001): A buried two-dimensional $c(2 \times 2)$ antiferromagnet

Jayanta Das,[1] Sananda Biswas,[2] Asish K. Kundu,[1] Shobhana Narasimhan,[2,3] and Krishnakumar S. R. Menon[1,*]
[1]*Surface Physics and Material Science Division, Saha Institute of Nuclear Physics, 1/AF Bidhannagar, Kolkata 700064, India*
[2]*Theoretical Sciences Unit, Jawaharlal Nehru Centre for Advanced Scientific Research, Jakkur, Bangalore 560064, India*
[3]*Sheikh Saqr Laboratory, ICMS, Jawaharlal Nehru Centre for Advanced Scientific Research, Jakkur, Bangalore 560064, India*
(Received 7 January 2015; published 27 March 2015)

The growth, morphology, and magnetic structure of ultrathin Cr films grown on a Ag(001) substrate are studied using low-energy electron diffraction (LEED), angle-resolved photoemission spectroscopy (ARPES), and *ab initio* density functional theory (DFT) calculations. The presence and temperature dependence of $c(2 \times 2)$ half-order spots in the LEED pattern, for low electron energies, along with the presence of characteristic Cr 3*d* bands in the ARPES spectra, confirm the existence of antiferromagnetic ordering for the Cr monolayer case. Our experiments are also consistent with the presence of a $p(1 \times 1)$ Ag overlayer on top of the Cr layer, suggesting the existence of a Ag/Cr/Ag(001) sandwich structure at the surface. Our DFT calculations confirm that this is the most favored geometric and magnetic structure of the system. The Cr layer is found to retain a "two-dimensional" character with enhanced Cr 3*d* magnetic moments, despite being buried below a Ag monolayer, due to the absence of significant hybridization between Cr 3*d* and Ag 4*d* electronic states. The coverage dependence of the magnetic ordering indicates a maximum ordering above the expected monolayer coverage, possibly due to intermixing between Ag and Cr atoms in the overlayer.

DOI: 10.1103/PhysRevB.91.125435 PACS number(s): 75.70.Rf, 68.55.−a, 68.43.Bc, 79.60.−i

I. INTRODUCTION

The recent emergence of the field of spintronics has led to renewed interest in the electronic and magnetic properties of surfaces and interfaces of ferromagnetic (FM) and antiferromagnetic (AFM) metals. The reduced dimensionality of such surface and interface systems leads to a host of interesting properties that could conceivably be exploited for device applications. For instance, theoretical *ab initio* density functional theory (DFT) studies by Freeman and Fu [1–3] and by Blügel *et al.* [4–6] have predicted a strong enhancement of magnetic moments on the surfaces of 3*d* transition metals, as well as their overlayers on noble-metal and other nonmagnetic substrates. As examples of this, calculations [4] have shown that late transition metal (Fe, Co, and Ni) overlayers on the Pd(001) surface prefer a FM $p(1 \times 1)$ configuration, whereas early transition metal (V, Cr, and Mn) overlayers favor an AFM $c(2 \times 2)$ spin superstructure. Moreover, due to the current demand for size reduction of spintronic devices, there is a search for novel materials with anisotropic magnetoresistance. It has been shown that not just FM, but also AFM materials could become promising candidates for this purpose [7,8]. While there have been a large number of experimental studies on the properties of two-dimensional (2D) FM overlayers, there has been relatively little exploration of 2D antiferromagnetism in such systems, primarily due to the experimental difficulties in detecting surface antiferromagnetism.

Among the transition metals, Cr is expected to be particularly sensitive to changes in coordination and symmetry, as it possesses a half-filled 3*d* band. Earlier *ab initio* DFT calculations have pointed out that one obtains enhanced magnetic moments (close to atomic moments) on Cr surfaces [1–3] and on Cr monolayers (MLs) on metal surfaces [4,5]. It has been found that the 2D electronic nature of a freestanding ML is essentially retained when the ML is deposited on a noble-metal substrate, as there is very little hybridization between the noble-metal *d* bands and Cr *d* states, leading to electronic isolation [1,5].

At first, Cr might appear to be an ideal candidate for epitaxial growth on Ag(001), for two reasons: (i) the nearest-neighbor separation in face-centered-cubic Ag (2.89 Å) is only about 0.3% more than the lattice constant of body-centered-cubic Cr (2.88 Å), and (ii) there is a large miscibility gap for the Cr-Ag binary system above the melting point, suggesting that intermixing and alloy formation may possibly be unfavorable also at the surface. These factors would tend to favor the epitaxial growth of Cr on Ag(001), with its ⟨100⟩ direction rotated 45° relative to the substrate, along with a sharp Cr-Ag interface with little intermixing. However, there is also an opposing factor, viz., the fact that the surface energy of Cr (=2400 mJ/m^2) is much higher than that of the Ag substrate (=1250 mJ/m^2) [9]; according to Bauer's criterion [10], a flat growth mode (surface wetting) is favored when the surface free energy of the deposited metal is sufficiently lower than the free energy of the substrate, under conditions of thermodynamic equilibrium. For this reason, instead of the growth of a flat Cr overlayer, one may have the growth of multilayer domains or islands or (if kinetic barriers can be overcome) the Cr layer may be buried under one or more Ag layers.

The results from previous experimental and theoretical studies on the deposition of Cr on Ag(001) have resulted in an accumulation of data that are quite contradictory and often puzzling, regarding the growth mode, the geometric structure of the films, and their magnetic properties. At low temperatures (100 K) growth proceeds via the hit-and-stick (random-deposition) mode, as has been shown experimentally [11,12]. On the other hand, very high temperatures (above 500 K) result in Cr agglomeration, as well as Ag segregation [13,14]. The room-temperature (RT) growth of sub-ML Cr films on Ag(001) has been extensively studied [11,15–17]; it has,

*krishna.menon@saha.ac.in

however, been found to result in poorly ordered films, with bilayer or multilayer Cr islands exposing a significant amount of the uncovered Ag substrate. However, it was experimentally observed by the group of Gewinner [15–22] that it was possible to grow a flat ML of Cr on the Ag(001) substrate under nonequilibrium growth conditions when the deposition was carried out at moderate substrate temperatures (430–450 K). Further, they were also able to observe weak but distinct $c(2 \times 2)$ superstructure spots in low-energy electron diffraction (LEED), with very different characteristics from those usually observed for ordered $c(2 \times 2)$ surface alloys. The weak intensity, energy dependence, and temperature dependence of the spots confirmed their origin as resulting from a surface AFM ordering of the Cr layer.

Studies using the inverse photoemission technique [23] provided evidence for the growth of a Cr ML on Ag(001), along with enhanced Cr magnetic moments, when the growth was carried out at 440 K. However, the authors of these studies were unable to observe $c(2 \times 2)$ LEED spots. Steadman *et al.* [11], using *in situ* surface x-ray diffraction, also found a growth mode at 430 K on Ag(001), in which Cr forms a flat ML structure, covered, however, with 1 ML of Ag. In contrast, scanning tunneling microscopy (STM) studies on the same system [13,14] did not support the existence of flat ML growth, observing instead Cr agglomeration up to a growth temperature of 440 K. The authors of these studies concluded from their detailed STM investigations [13,14] that the growth of a perfectly flat ML film of Cr is not possible on the Ag(001) surface. However, it is worth noting that they too could not observe the $c(2 \times 2)$ superstructure LEED spots from these Cr ML surfaces. This runs contrary to claims that the initial mode of formation of the flat ML is largely determined by in-plane AFM interactions stabilizing the Cr in a metastable ML configuration, suggesting that one should expect flat Cr MLs to occur only in the presence of long-range in-plane AFM interactions. A large part of these temperature-dependent differences in growth mode and structure presumably arise because the mobility of the Cr atoms is enhanced as the growth temperature is increased. The possibility of some degree (about 20%–30%) of intermixing between Cr and Ag has also been postulated in the literature [11,12], due to the far-from-equilibrium growth mode. The experimental observation of Ag segregation on Cr ML films, even at moderate temperatures, has also been reported [20], supported by STM [14] and surface x-ray diffraction [11] studies.

Regarding the magnetic properties, various authors have reported both high and low moments on the Cr atoms and either FM or AFM ordering. Some of this confusion may arise from the variety of growth modes that have been observed, since the geometric and magnetic structures are intimately connected. Early photoemission experiments by Newstead *et al.* [24] indicated an enhancement of Cr moments that was much less than that predicted by calculations, as well as a rapid reduction of moments with an increase in Cr coverage. Polarized neutron reflection measurements performed by Johnson *et al.* [25] on a 0.33-ML Cr film in a Ag/Cr/Ag(001) multilayer stack reportedly indicated long-range FM order, with a Cr moment consistent with theoretical predictions. The observation of coherently exchange-scattered half-order spots in LEED confirmed the existence of a $c(2 \times 2)$ AFM ground state for the flat Cr ML grown on Ag(001) at moderate substrate temperatures (430–450 K), as reported by the group of Gewinner [15–22], marking a significant step in the exploration of 2D AFM systems. However, in spite of rigorous studies using different surface sensitive techniques, they were not able to come to a conclusion on the exact structure of the Cr ML on Ag(001). Moreover, the inability of other groups to reproduce the $c(2 \times 2)$ AFM LEED spots also raised some doubts about the validity of these results, as well as about the geometric and magnetic structure of Cr/Ag(001).

Given the variations in the experimental observations made in earlier studies, and the discrepancies in some cases between experiment and theory, we feel it is worthwhile to re-examine the flat ML growth of Cr on Ag(001). In this paper, we present results from a combined experimental and theoretical study of the growth and structural aspects of ultrathin Cr films on a Ag(001) substrate deposited at 428 K. Our combination of LEED and photoemission experiments confirms the presence of AFM order at the surface and probes the Cr coverage dependence of magnetic long-range ordering in the system. In agreement with our experimental results, our *ab initio* DFT studies show that the stable surface structure of the system consists of the Cr layer being buried one layer deep, i.e., under one atomic layer of Ag. They also confirm that the magnetic ground state of the system is a $c(2 \times 2)$ AFM configuration.

II. EXPERIMENTAL DETAILS

A well-ordered Ag(001) surface was prepared by repeated cycles of Ar ion sputtering (600 eV, 1 μA) for 15 min, followed by annealing to 823 K for 30 min, until a sharp $p(1 \times 1)$ LEED pattern was observed. Cr was evaporated from a high-purity (99.95%) Cr rod, kept in a water-cooled electron-beam evaporator in the preparation chamber, at a rate of 0.2 Å/min, calibrated with a quartz crystal thickness monitor. A ML is defined as an atomic density of 1.2×10^{19} atoms/m^2, corresponding to that of the Ag(001) surface. The chamber pressure was maintained below 2×10^{-10} mbar during Cr deposition. Cr films of various coverages were grown on the Ag(001) substrate in single-step mode, i.e., for each coverage study, a fresh substrate was prepared and a fresh film was grown with the desired coverage. Further details of the growth optimization and characterization can be found elsewhere [26]. In the case of high-temperature growth, the substrate temperature was brought down to RT immediately after Cr deposition. LEED measurements were performed using a four-grid LEED apparatus (OCI Vacuum Microengineering), to determine the crystalline quality of the deposited film, as well as the crystallographic symmetry directions. A highly-sensitive Peltier-cooled 12-bit CCD camera was used to collect LEED images, with software controlling the gain/exposure settings of the camera, as well as all the other controls of the LEED instrument.

The x-ray photoemission spectroscopy (XPS) and angle-resolved photoemission spectroscopy (ARPES) measurements were performed in the analysis chamber with a base pressure lower than 8×10^{-11} mbar. ARPES measurements were performed using a combination of VG Scienta-R4000WAL

electron energy analyzer with a 2D CCD detector, and a high-flux Gammadata VUV He lamp attached to a VUV monochromator, which have been described in detail elsewhere [27]. We used the He I_α (21.218-eV) resonance line to excite the photoelectrons from the sample surface for the ARPES measurements, while an Al K_α monochromatic x-ray source (1486.6 eV) from VG Scienta was used for XPS measurements. All ARPES and XPS measurements were performed at RT, with total experimental energy resolutions better than 0.1 and 0.65 eV, respectively. The coverages of the deposited Cr films were estimated from the XPS intensity measurements and were in good agreement with the quartz crystal thickness monitor calibrations. Temperature-dependent LEED measurements were performed while warming up the sample, after cooling it down to 100 K using liquid nitrogen. The experiments were repeated several times, and we have thus confirmed the reproducibility of all the results presented below.

III. COMPUTATIONAL DETAILS

The calculations were performed using spin-polarized DFT as implemented in the PWSCF code of the QUANTUM ESPRESSO distribution [28]. A plane-wave basis set was used to expand the Kohn-Sham equations, with cutoffs of 40 and 400 Ry for wave functions and charge densities, respectively. Ultrasoft pseudopotentials [29] were used to describe the interactions between the valence electrons and the ionic cores. A generalized gradient approximation of the Perdew-Burke-Ernzerhof form [30] was used to approximate the exchange-correlation functional.

A 15-atomic-layer-thick slab was used to model the Ag(001) surface. We have considered four atomic configurations for Cr deposited on Ag(001), with Cr MLs placed symmetrically on both the top and the bottom surfaces of a 17-atomic-layer thick slab: (i) Cr/Ag(001), with a Cr ML as the outermost surface layer on either side of the slab; (ii) 1Ag/Cr/Ag(001), where the Cr ML is buried under one atomic layer of Ag; (iii) 2Ag/Cr/Ag(001), where the Cr ML is buried under two atomic layers of Ag; and (iv) 3Ag/Cr/Ag(001), where the Cr ML is buried under three atomic layers of Ag. In all cases, the stacking was assumed to follow the ABAB . . . stacking characteristic of the face-centered-cubic (fcc) structure along the [001] direction.

The in-plane lattice constant was fixed at 2.94 Å $= (1/\sqrt{2})$ of the theoretically obtained value of the bulk lattice constant of Ag, which is in very good agreement with the previously reported value of Cipriani *et al.* [31]. All atomic layers, except the middle three layers of the slab, were allowed to relax, so as to obtain an optimized geometry. The Broyden-Fletcher-Goldfarb-Shanno (BFGS) algorithm was used to move atomic coordinates until the forces on the relaxed atoms were less than 0.001 Ry/bohr along each Cartesian direction. Brillouin-zone sums were carried out using Monkhorst-Pack meshes [32] that were approximately commensurate with a $17 \times 17 \times 1$ sampling for the (1×1) surface unit cell, along with Marzari-Vanderbilt smearing [33] with a width of 0.001 Ry.

IV. EXPERIMENTAL RESULTS

Here, we present the experimental results from LEED and ARPES investigations of Cr grown on Ag(001) at RT and at 428 K. Figures 1(a) and 1(b) show the LEED pattern of a 1-ML Cr film deposited on Ag(001) at RT, for primary electron energies (E_p) of 40 and 23 eV, respectively, while Figs. 1(c) and 1(d) show the corresponding patterns for a 1-ML Cr film deposited at 428 K. The sharp first-order [1, 0] LEED spots are distinctly visible in Fig. 1(a) and the corresponding first surface Brillouin zone is also drawn in the same figure, indicating some high-symmetry points. The LEED pattern clearly changes for a Cr ML grown at 428 K [see Fig. 1(c)], where, along with the $p(1 \times 1)$ LEED spots (broadened due to the increased contrast level), we observe a $c(2 \times 2)$ superstructural pattern (enclosed in white circles) which is absent in the RT-grown sample

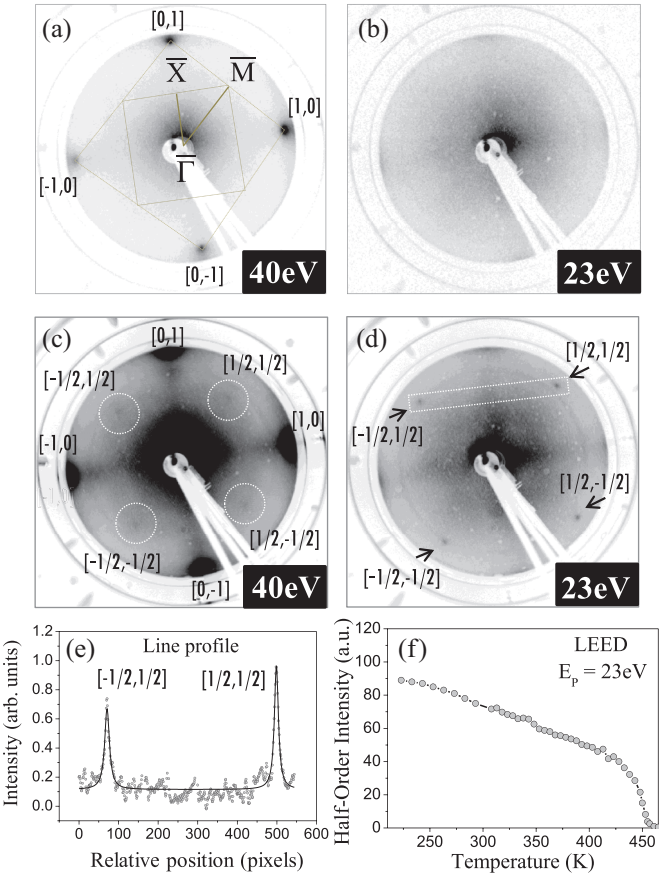

FIG. 1. (Color online) (a) LEED pattern for 1 ML of Cr deposited on Ag(001) at RT, for a primary electron energy E_p of 40 eV, indicating sharp $p(1 \times 1)$ spots. The surface Brillouin zone and corresponding high-symmetry directions are marked. (b) LEED pattern for $E_p = 23$ eV at RT, showing the absence of half-order spots. (c) LEED pattern for 1 ML of Cr deposited on Ag(001) at 428 K ($E_p = 40$ eV), showing weak $c(2 \times 2)$ half-order spots (enclosed in white circles), along with integer-order spots. (d) For $E_p = 23$ eV, clear half-order spots are shown. (e) Line profile along the half-order spots $(-1/2, 1/2)$ and $(1/2, 1/2)$ [boxed region in (d)]. (f) Average intensity variation of the half-order spots at 23 eV (E_p), as a function of the sample temperature, confirming AFM order with a transition temperature of ∼450 K.

[Fig. 1(a)]. The intensity of these $c(2 \times 2)$ spots is enhanced as the energy is lowered and reaches a maximum at 23 eV [see Fig. 1(d)], though at this beam energy the integer-order spots do not enter the field of view of the LEED screen. These "extra" spots with a weak intensity have coordinates [1/2, 1/2] and are called "half-order" spots; they were only detectable up to about 60 eV in our setup. The intensities of these half-order spots are only about 2% those of the first-order integer spots, at the respective energies of their intensity maxima (i.e., at 23 and 55 eV) at RT, normalized to the respective electron-beam currents. A line profile over the $(-1/2, 1/2)$ and $(1/2, 1/2)$ half-order spots [see the boxed region in Fig. 1(d)] is shown in Fig. 1(e). The temperature dependence of the intensity (averaged over four half-order LEED spots) has been measured within the range of 225 to 450 K, at an electron energy of 23 eV; these results are shown in Fig. 1(f). The half-order LEED intensity is found to decrease with an increase in temperature, eventually vanishing above a transition temperature of ~450 K.

These half-order spots are similar to those observed by Krembel *et al.* for the Cr/Ag(001) system [15,16]; similar observations have also been made in the case of NiO [34,35], where it is well established that these half-order spots originate due to exchange interactions between the low-energy electrons and the AFM Cr/Ni surface moments. In the present case also, the observed weak intensity of the half-order spots compared to that of the integral spots, their diminishing intensity with increasing electron energy, and the temperature dependence of these half-order spots all confirm their AFM origin and rule out other possibilities, such as the formation of ordered $c(2 \times 2)$ surface alloys or the displacive reconstruction of the top layers [15,16]. Thus, the observation of $c(2 \times 2)$ half-order spots confirms the in-plane AFM arrangement of the Cr moments in the Cr ML grown at 428 K, in contrast to that grown at RT.

We have optimized the growth conditions for obtaining a well-ordered flat Cr ML grown on Ag(001); for a growth temperature of 428 K, the Cr ML is found to have the highest degree of AFM ordering, and this is employed in the present experiments for further study of the dependence on Cr coverage [26]. The average half-order spot intensities of Cr films measured at RT for different Cr coverages, at a beam energy of 23 eV, are plotted in Fig. 2(a). At a coverage of 0.2 ML, the half-order spots are hardly visible. The fourfold half-order spots are observed with a weak intensity within the sub-ML coverage range of 0.5–0.8 ML, whereas the spot intensity becomes distinctly visible for the Cr coverage range of 1.0–1.5 ML, with the maximum intensity being achieved for a film coverage of about 1.2 ML. The intensity of the half-order spots starts to diminish above 1.6 ML and almost vanishes at close to 2-ML Cr coverage. These results were found to be highly reproducible. Interestingly, we find that our experimental data for the intensity of the half-order spots as a function of the film coverage can be fitted reasonably well by a Gaussian [see the thin solid line in Fig. 2(a)].

In Fig. 2(b), we show the ARPES spectra obtained at the $\overline{\mathrm{M}}$ point in the $p(1 \times 1)$ surface Brillouin zone using He I_α photons, from Cr/Ag(001) films grown at 428 K, for different Cr coverages. For comparison, we also show the spectra obtained for bare Ag(001). Ag does not have any bands

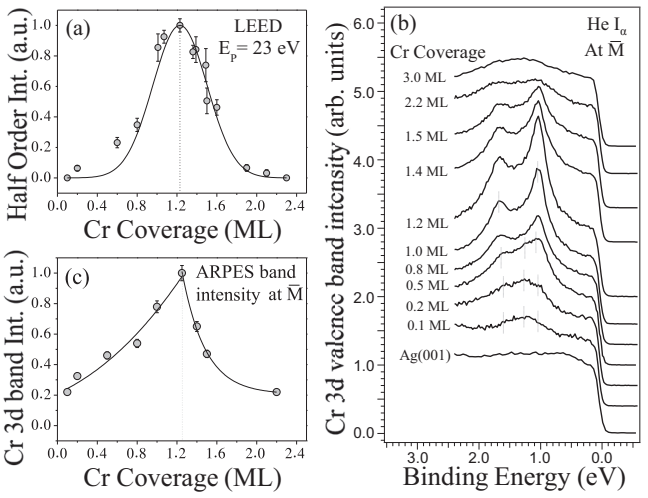

FIG. 2. (a) Average intensity of $c(2 \times 2)$ half-order spots (for $E_p = 23$ eV) measured at RT from Cr deposited on Ag(001), for a deposition temperature of 428 K, as a function of the film coverage. Error bars indicate intensity variations for different half-order spots. (b) ARPES spectra at the $\overline{\mathrm{M}}$ point measured at RT using He I_α, showing the emergence of AFM Cr 3*d* bands as a function of Cr coverage. (c) Variation of the extracted Cr 3*d* band intensity from (b), for different Cr coverages, with a deposition temperature of 428 K.

present in this energy range and shows only a smooth and flat background. The twin peaks (bands) observed with growing Cr coverage correspond to Cr 3*d* bands, and their origin has been attributed to an in-plane Cr-Cr AFM interaction [12,22,36]. However, for low Cr coverages (below 0.5 ML), we observe broad Cr 3*d* bands with features at binding energies (BEs) of about 1.05, 1.25, and 1.6 eV [indicated by thin vertical lines in Fig. 2(b)]. As the coverage increases, the feature at 1.25 eV decreases in intensity and vanishes above 0.5-ML coverage, whereas the features at 1.05 and 1.6 eV increase in intensity and evolve into distinct bands for 0.5 ML and above. The intensities of these two well-resolved bands increase with further increases in Cr coverage and reach a maximum for about 1.2-ML coverage, after which they decrease, then vanish above 2.2-ML coverage. The dispersion of the feature at 1.25 eV (not shown) closely follows the dispersion of the Cr 3*d* AFM band features (at 1.05 and 1.6 eV) and can be considered to be arising from in-plane Cr-Cr AFM interactions. The coverage dependence of the intensity, as well as the BE position, of the feature at 1.25 eV probably indicates that these states originate from the edge Cr atoms of $c(2 \times 2)$ Cr ML islands, whose contribution to the photoemission spectra decreases as the island size increases with increasing Cr coverage.

The normalized Cr 3*d* AFM band intensities extracted from Fig. 2(b) are plotted in Fig. 2(c) against the respective Cr coverages; the thin solid line is a guide for the eye. As expected, the overall nature of the Cr 3*d* band intensities in Fig. 2(c) is similar to that of the LEED half-order intensities [in Fig. 2(a)], with the maximum intensity occurring at about 1.2-ML Cr coverage. However, the shape of the curve is very different from that obtained for the LEED data, possibly due to a difference in the correlation lengths between these two

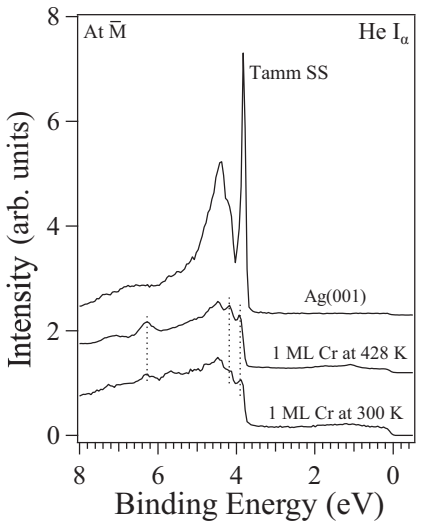

FIG. 3. ARPES spectra at the $\bar{M}$ point in the surface Brillouin zone, over a wide binding energy range, using He I_α, for the cases of bare Ag (001), 1 ML of Cr deposited at 428 K, and 1 ML of Cr deposited at RT. See text for details.

techniques. For Cr coverages of 3 ML and above, the Cr 3*d* band structure suggests a paramagnetic state [37].

ARPES spectra obtained from the clean Ag(001) surface, and from 1 ML Cr on Ag(001) (grown at 428 K and RT), at the $\bar{M}$ point in the surface Brillouin zone, using He I_α photons over a wider BE region, are shown in Fig. 3. The sharp peak at a BE of 3.9 eV for clean Ag(001) is the well-known Tamm-like surface state at $\bar{M}$. Upon deposition of Cr, the intensity of this surface state nearly vanishes when Cr covers almost the entire Ag surface. This is the case for Cr films deposited at both 428 K and RT, although the weak structure prevailing at the surface state position is attributed to a bulk transition [38]. The intensity of the Ag bulk 4*d* states (above 4-eV BE) gets suppressed in the ARPES spectra for 1 ML Cr, due to the presence of the Cr overlayer. There are still major differences in the spectra of the RT vs 428 K samples: we observe two features, at 4.2 and 6.3 eV (marked in Fig. 3), for the 428 K sample, which are quite weak for the RT sample. Segregation of Ag atoms on top of the Cr film is a possibility, due to the lower surface energy of the Ag surface; this phenomenon has been studied for the RT grown Cr/Ag(001) system [12,20]. The feature at 6.3 eV is known to be a characteristic signature of the presence of segregated Ag on the surface and does not arise from the Ag(001) substrate underneath [12,20]. The significant intensity of this 6.3-eV feature observed for the 428 K sample, in comparison to the RT sample (see Fig. 3), suggests that there is much segregation of Ag onto the 1-ML Cr film grown at higher temperatures, as expected. A growth study by Steadman *et al.* [11], using *in situ* surface x-ray diffraction for a Cr ML grown at 430 K, suggested that the Cr layer is covered by a layer of Ag atoms, consistent with our observations. We also observe that the 4.2-eV feature has a dispersion similar to that of the Tamm surface state on the clean Ag(001) surface but is shifted to a higher BE by about 0.3 eV. This new Tamm-like surface state appears to be originating from a Ag layer on top of the Cr ML film with (1×1) ordering but is shifted to a higher BE due to the different surface potential on the Cr film [12,15]. Thus, the observation of the 4.2-eV feature for the film grown at 428 K (see Fig. 3) indicates the presence of a Ag(001) layer segregated on top of the Cr ML film; we show below that this conclusion is corroborated by our *ab initio* DFT calculations.

V. COMPUTATIONAL RESULTS

In our *ab initio* DFT calculations, we search for the thermodynamically most favorable structural and magnetic configuration. Note, however, that in an actual experimental scenario, kinetic barriers could possibly prevent the system from achieving this ground-state structure. We have considered system geometries in which the Cr layer either is the overlayer or is buried under 1, 2, or 3 MLs of Ag. For the magnetic structure, we restrict ourselves to consideration of two collinear magnetic configurations: the $p(1 \times 1)$ FM one and a $c(2 \times 2)$ AFM one. Table I lists our results for the energetics and magnetic moments in the eight configurations considered. From this table, we see that the most favored configuration is AFM 1Ag/Cr/Ag(001). However, AFM 2Ag/Cr/Ag(001) is almost degenerate with this, lying only 18 meV/Cr atom higher in energy. This finding supports our experimental results (presented in the previous section) for the growth of Cr on Ag(001) at 428 K, as well as the results of a previous growth study at 430 K by Steadman *et al.* [11], using *in situ* surface x-ray diffraction.

Figures 4(a) and 4(b) show top and side views of the most favored AFM 1Ag/Cr/Ag(001) structure. In Fig. 4(c) we display the interlayer relaxations, where $\Delta_{ij} \equiv [(d_{ij} - d_b)/d_b] \times 100$; here, d_{ij} is the interlayer spacing between layer i and layer j, and d_b is the bulk interlayer spacing.

Upon examining our results for magnetic moments in Table I, we see that the Cr atoms retain a significantly high spin moment, even when they are buried under one or more layers of Ag. The reason for this is that there is very little overlap between the electronic density of states of Cr atoms and that of Ag atoms and, therefore, very little Cr-Ag hybridization. This is evident in Fig. 5, where we plot the spin-resolved projected density of states for Cr 3*d* states, as well as the 4*d* states of Ag atoms in the first and third layers. The reduced atomic coordination of the Ag atoms in the first layer results

TABLE I. Results from DFT calculations for the energetics of various ferrromagnetic (FM) and $c(2 \times 2)$ antiferromagnetic (AFM) configurations of Cr on Ag(001) systems studied here. ΔE denotes the energy of a given configuration with respect to the lowest energy configuration, i.e., the AFM configuration of 1Ag/Cr/Ag(001). m_{Cr} is the magnetic moment per Cr atom in the given system.

	Results for magnetic structures			
	FM		AFM	
System	ΔE (meV/Cr atom)	$m_{\mathrm{Cr}}^{\mathrm{FM}}$ (μ_B)	ΔE (meV/Cr atom)	$m_{\mathrm{Cr}}^{\mathrm{AFM}}$ (μ_B)
Cr/Ag(001)	797	4.71	475	4.46
1Ag/Cr/Ag(001)	393	4.19	0	4.36
2Ag/Cr/Ag(001)	463	4.20	18	4.29
3Ag/Cr/Ag(001)	456	4.20	62	4.32

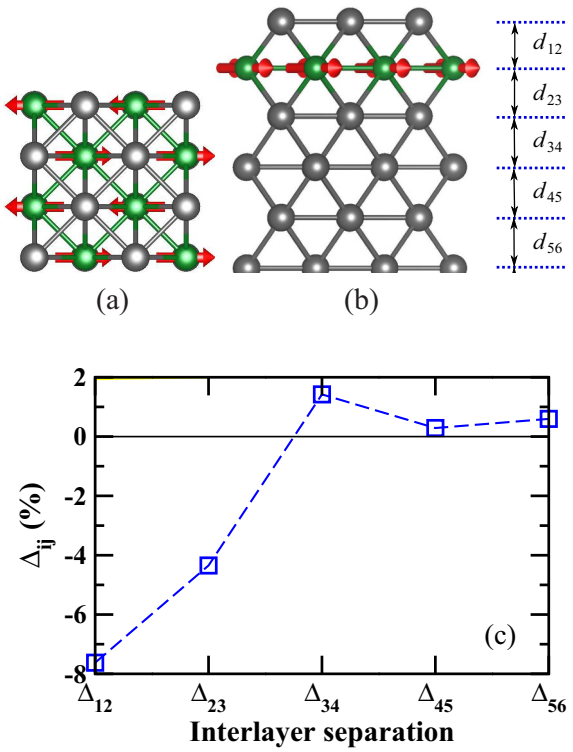

FIG. 4. (Color online) Geometry of the energetically most favored structure, $c(2 \times 2)$ AFM 1Ag/Cr/Ag(001): (a) top and (b) side views of the system. Light-gray and dark-gray (green) spheres represent Ag and Cr atoms, respectively. The (red) arrows indicate the directions of spins. Note that in the absence of spin-orbit interactions, the in-plane and out-of-plane spin directions are equivalent. (c) Δ_{ij}, the percentage change in interlayer separations, for the first few surface layers. See text for the definition of Δ_{ij} and (b) for the convention used in numbering layers.

in the reduction of the Ag 4*d* bandwidth for atoms in this layer, as is clearly shown in Fig. 5. Note also the clear spin polarization of the Cr atoms. Upon performing a calculation for an isolated ML of Cr atoms, maintained at the same in-plane

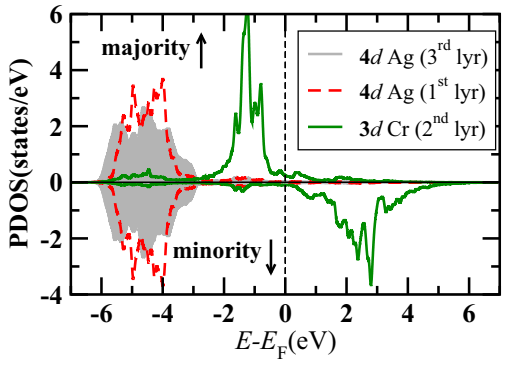

FIG. 5. (Color online) Theoretically calculated results for the spin-polarized projected density of states (PDOS) of 1Ag/Cr/Ag(001) in the $c(2 \times 2)$ AFM configuration. Dashed (red) line, PDOS from first-layer Ag 4*d* states; solid (green) line, PDOS from second-layer Cr 3*d* states; and shaded (gray) area, PDOS from third layer Ag 4*d* states.

lattice constant, in the $c(2 \times 2)$ AFM configuration, we obtain a magnetic moment per Cr atom of $4.45\mu_B$. Thus, we see that when Cr is present as an overlayer on the Ag(001) substrate, the magnetic moment on Cr atoms is essentially unchanged, and it is only very slightly reduced when the Cr layer is buried. For Cr/Ag(001) our value of $m_{\mathrm{Cr}}^{\mathrm{AFM}} = 4.46\mu_B$ is larger than the previously reported [5] value of $\sim 3.8\mu_B$; we believe that the main reason for this discrepancy is that the interlayer spacings were not optimized in this very early previous calculation.

VI. DISCUSSION

The structure and properties of Cr ML on a Ag(001) substrate are strongly dependent on the deposition conditions and initial growth mode. Considerations of surface free energy [that for Cr(001) is almost double the value for Ag(001)] would suggest that one should obtain the formation of multilayer Cr islands, so as to minimize the surface area; this occurs for deposition at RT. However, for deposition at higher temperatures (430–450 K), both the Cr and the Ag atoms have a higher mobility, enabling them to achieve the thermodynamically most favorable configuration, in which the Cr atoms are buried below one layer of Ag atoms and form a flat ML film with $c(2 \times 2)$ ordering. Thus, the minimum energy configuration of the system is found to be a sandwich structure of 1 ML Ag/1 ML Cr/Ag(001), consistent with our experimental observations as well as with our *ab initio* DFT calculations.

Our observation of $c(2 \times 2)$ half-order spots in LEED is direct proof of the surface AFM ordering of the Cr ML film on the Ag(001) substrate. However, the presence of a Ag overlayer covering the Cr ML will attenuate the half-order LEED intensity originating from the Cr layer. This is probably the reason that the observed relative intensity of the half-order LEED spots in our case (1%–12%) is less than the theoretically estimated value of 2%–4% for an AFM Cr plane on Pd(0001) [39]. In a previous study of Cr ML growth at 430 K by Hanf *et al.* [12], the authors debated the presence of a Ag overlayer on the ML Cr film. However, they concluded that the surface consisted of coexisting $p(1 \times 1)$ Ag patches and AFM $c(2 \times 2)$ Cr ML platelets, with the half-order intensities originating only from the Cr ML platelets. They observed a reduction of $\sim$75% in the half-order spot intensity when 1 ML of Ag was further deposited at RT on top of 1 ML Cr grown at 430 K [12], based on which they concluded that below the $p(1 \times 1)$ Ag layer, a $c(2 \times 2)$ AFM Cr layer cannot be formed. However, our *ab initio* DFT calculations (see Table I) indeed show that a $c(2 \times 2)$ AFM Cr layer buried below a Ag ML is the most stable configuration, also in agreement with the *in situ* growth studies by Steadman *et al.* [11].

A further deposition of 1 ML Ag onto the 1Ag/Cr/Ag(001) system is not expected to destabilize the AFM ordering of the Cr layers, as the 2Ag/Cr/Ag(001) and 1Ag/Cr/Ag(001) configurations are found to be nearly degenerate (see Table I). However, a strong reduction in intensities of the half-order spots is expected, due to the stronger attenuation of the magnetically scattered electrons by the thicker Ag layers.

In Fig. 2(a), we observe a detectable half-order LEED intensity only above a coverage of 0.5 ML. Below this coverage, the weak half-order spots are difficult to distinguish

from the diffused background observed in LEED due to scattering from defects and other surface imperfections. A similar observation led Hanf *et al.* [12] to conclude that below a coverage of 0.3 ML, the AFM $c(2 \times 2)$ domains do not form at all. They concluded that the Cr $c(2 \times 2)$ domains just begin to nucleate below a coverage of 0.7 ML, and the Cr atoms grow in ML $c(2 \times 2)$ domains only above a coverage of 0.7 ML. At the coverage corresponding to the maximum intensity of half-order spots, they suggested that the flat Cr ML film is in fact inhomogeneous, with the coexistence of Cr ML patches along with an Ag coated Cr-Ag alloy. This conclusion was based on the assumption that below the $p(1 \times 1)$ Ag overlayer, a stable $c(2 \times 2)$ Cr layer with AFM order cannot be formed. However, our *ab initio* DFT calculations have shown that a Cr ML buried under Ag layers still retains the $c(2 \times 2)$ AFM structure, without much reduction in the Cr magnetic moments. Moreover, from the experiments we have carried out for different Cr coverages, we observe that ARPES measurements are more sensitive to AFM ordering [the presence of Cr 3*d* AFM bands with $c(2 \times 2)$ symmetry] than LEED (AFM half-order spots) measurements. In the case of ARPES, the Cr 3*d* AFM bands are present in a BE region where only weak Ag *sp* bands are present and can therefore be detected more easily. We note that our ARPES experiments clearly indicate the presence of AFM bands for Cr coverages as low as 0.1 ML [see Fig. 2(c)]. From the coverage dependence of the Cr 3*d* AFM band intensity in Fig. 2(c), it clear that the $c(2 \times 2)$ domains are formed even for very low coverages of Cr on Ag(001) at 428 K and grow in size in a percolative way with increasing Cr coverage, until the intensity reaches a maximum. Upon further deposition, the 2D nature of the Cr film is lost as a second Cr layer begins to grow with a reduced nearest-neighbor distance (2.49 Å instead of 2.88 Å), decreasing the $c(2 \times 2)$ AFM domain size with increasing coverage. Thus, our experiments and calculations point to the formation of Cr ML domains coated with ML of Ag from the very initial stages of growth on Ag(001) at 428 K and do not support the presence of mixed phases of $p(1 \times 1)$ Ag patches along with $c(2 \times 2)$ Cr ML patches as proposed earlier [12]. Our results are also compatible with the observation of Ag islands in STM [13,14], as the deposited Cr atoms have now interchanged their positions with Ag atoms, and the topmost layer is still populated by Ag atoms.

It is interesting to note that the maximum intensity of the half-order LEED spots, as well as the AFM Cr 3*d* bands, is observed to occur for a coverage of about 1.2 ML (see Fig. 2), instead of at the expected completion of a single ML (1 ML) of Cr. This is found to be reproducible in our different growth experiments and is in agreement with the literature [12]. To explain this observation, we note that Steadman *et al.*, in their earlier detailed growth study [11], found that for growth at 430 K, there was an intermixing of about 22% between the Cr atoms and the top-layer Ag atoms. Thus, in the case of 1-ML Cr coverage, 22% of the top Ag layer is occupied by Cr atoms, while only 78% of the buried Cr layer is occupied by Cr atoms. Upon depositing more Cr atoms, it appears that more Cr atoms have diffused into the buried Cr layer, increasing the occupancy of Cr atoms in the second layer. Thus, for a coverage of 1.2 ML, the Cr layer has a maximum Cr occupation, leading to a maximum strength of the in-plane AFM interaction and, therefore, maxima in the intensities of the half-order spots in LEED and AFM bands in ARPES.

VII. CONCLUSIONS

We have revisited the question of the growth of a Cr ML on a Ag(001) substrate and have provided both experimental and theoretical confirmation that the thermodynamically most stable structure of this system consists of an antiferromagnetically ordered flat Cr ML film buried under a layer of Ag atoms.

Experimentally, we have found that at an optimum growth temperature of 428 K, the signature of the AFM ordering is clearly observed in the LEED images as a weak $c(2 \times 2)$ superstructure, which is observed only at low energies (below 60 eV) and found to vanish above a transition temperature of $\sim$450 K. Further proof of the AFM ordering in the Cr ML is the observation of Cr 3*d* bands with $c(2 \times 2)$ symmetry in the ARPES spectra of the system. The intensity of these Cr 3*d* bands closely follows the half-order spot LEED intensity as a function of the Cr coverage, with a maximum at a Cr coverage of 1.2 ML, suggesting a small intermixing of Cr and Ag atoms in the topmost layer.

Our LEED and ARPES data suggest that the $c(2 \times 2)$ AFM domains are formed from the very early stages of growth of Cr on Ag(001), at 428 K. This suggests that the Ag/Cr/Ag(001) sandwich structure is present from the initial stages of growth, in agreement with the observation of Ag steps in STM studies but running counter to an earlier suggestion that the system consists of an inhomogeneous surface with coexisting patches of (1×1) Ag and $c(2 \times 2)$ Cr ML platelets. Further detailed microscopic studies are necessary to obtain a better understanding of these issues.

ACKNOWLEDGMENTS

We acknowledge the Micro-Nano initiative program of the Department of Atomic Energy, Government of India, for generous funding and support. S.B. acknowledges CSIR, India, for a research fellowship.

[1] A. J. Freeman and C. L. Fu, J. Appl. Phys. **61**, 3356 (1987).
[2] C. L. Fu and A. J. Freeman, Phys. Rev. B **33**, 1755 (1986).
[3] C. L. Fu, A. J. Freeman, and T. Oguchi, Phys. Rev. Lett. **54**, 2700 (1985).
[4] S. Blügel, M. Weinert, and P. H. Dederichs, Phys. Rev. Lett. **60**, 1077 (1988).
[5] S. Blügel, B. Drittler, R. Zeller, and P. H. Dederichs, Appl. Phys. A **49**, 547 (1989).
[6] S. Blügel, Phys. Rev. Lett. **68**, 851 (1992).

[7] A. B. Shick, S. Khmelevskyi, O. N. Mryasov, J. Wunderlich, and T. Jungwirth, Phys. Rev. B **81**, 212409 (2010).
[8] B. G. Park, J. Wunderlich, X. Martí, V. Holý, Y. Kurosaki, M. Yamada, H. Yamamoto, A. Nishide, J. Hayakawa, H. Takahashi, A. B. Shick, and T. Jungwirth, Nat. Mater. **10**, 347 (2011).
[9] C. Krembel, M. C. Hanf, P. Wetzel, C. Pirri, J. C. Peruchetti, D. Bolmont, and G. Gewinner, Vacuum **41**, 460 (1990).
[10] E. Bauer, Z. Kristallogr. **110**, 372 (1958).
[11] P. Steadman, C. Norris, C. L. Nicklin, N. Jones, J. S. G. Taylor, S. A. de Vries, and S. L. Bennett, Phys. Rev. B **64**, 245412 (2001).
[12] M. C. Hanf, C. Krembel, and G. Gewinner, Surf. Sci. **519**, 1 (2002).
[13] J. F. Lawler, R. G. P. van der Kraan, H. van Kempen, and A. J. Quinn, J. Magn. Magn. Mater. **165**, 195 (1997).
[14] A. J. Quinn, J. F. Lawler, R. Schad, and H. van Kempen, Surf. Sci. **385**, 395 (1997).
[15] C. Krembel, M. C. Hanf, J. C. Peruchetti, D. Bolmont, and G. Gewinner, Phys. Rev. B **44**, 8407 (1991).
[16] C. Krembel, M. C. Hanf, J. C. Peruchetti, D. Bolmont, and G. Gewinner, J. Magn. Magn. Mater. **119**, 115 (1993).
[17] D. Rouyer, C. Krembel, M. C. Hanf, D. Bolmont, and G. Gewinner, Surf. Sci. **287–288**, 935 (1995).
[18] P. Schieffer, C. Krembel, M.-C. Hanf, G. Gewinner, and Y. Gauthier, Phys. Rev. B **65**, 235427 (2002).
[19] M. C. Hanf, C. Krembel, D. Bolmont, and G. Gewinner, Phys. Rev. B **68**, 144419 (2003).
[20] C. Krembel, M. C. Hanf, J. C. Peruchetti, D. Bolmont, and G. Gewinner, J. Vac. Sci. Technol. A **10**, 3325 (1992).
[21] C. Krembel, M. C. Hanf, J. C. Peruchetti, D. Bolmont, and G. Gewinner, Surf. Sci. **269–270**, 748 (1992).
[22] C. Krembel, M. C. Hanf, J. C. Peruchetti, D. Bolmont, and G. Gewinner, Phys. Rev. B **44**, 11472 (1991).
[23] J. E. Ortega and F. J. Himpsel, Phys. Rev. B **47**, 16441 (1993).
[24] D. A. Newstead, C. Norris, C. Ninns, and P. C. Stephenson, J. Phys. C: Solid State Phys. **20**, 6245 (1987).
[25] A. D. Johnson, J. A. C. Bland, C. Norris, and H. Lauter, J. Phys. C **21**, L899 (1988).
[26] J. Das, A. K. Kundu, and K. S. R. Menon, Vacuum **112**, 5 (2015).
[27] S. K. Mahatha and K. S. R. Menon, Curr. Sci. **98**, 759 (2010).
[28] See http://www.quantum-espresso.org for Quantum-ESPRESSO package; P. Giannozzi *et al.*, J. Phys.: Condens. Matter **21**, 395502 (2009).
[29] D. Vanderbilt, Phys. Rev. B **41**, 7892 (1990).
[30] J. P. Perdew, K. Burke, and M. Ernzerhof, Phys. Rev. Lett. **77**, 3865 (1996).
[31] G. Cipriani, D. Loffreda, A. Dal Corso, S. de Gironcoli, and S. Baroni, Surf. Sci. **501**, 182 (2002).
[32] H. Monkhorst and J. Pack, Phys. Rev. B **13**, 5188 (1976).
[33] N. Marzari, D. Vanderbilt, A. De Vita, and M. C. Payne, Phys. Rev. Lett. **82**, 3296 (1999).
[34] P. W. Palmberg, R. E. DeWames, and L. A. Vredevoe, Phys. Rev. Lett. **21**, 682 (1968).
[35] K. S. R. Menon, S. Mandal, J. Das, T. O. Menteş, M. A. Niño, A. Locatelli, and R. Belkhou, Phys. Rev. B **84**, 132402 (2011).
[36] G. Allan, Phys. Rev. B **44**, 13641 (1991).
[37] J. Das, A. K. Kundu, and K. S. R. Menon (unpublished).
[38] A. Goldmann and E. Bartels, Surf. Sci. **122**, L629 (1982).
[39] E. Tamura, S. Blügel, and R. Feder, Solid State Commun. **65**, 1255 (1988).